

Non-Fermi Liquid Behavior Close to a Quantum Critical Point in a Ferromagnetic State without Local Moments

E. Svanidze,¹ L. Liu,² B. Frandsen,² B. D. White,³ T. Besara,⁴ T. Goko,^{2*} T. Medina,⁵ T. J. S. Munsie,⁵
G. M. Luke,⁵ D. Zheng,⁶ C. Q. Jin,⁶ T. Siegrist,⁴ M. B. Maple,³ Y. J. Uemura,² and E. Morosan¹

¹Department of Physics and Astronomy, Rice University, Houston, TX 77005 USA

²Department of Physics, Columbia University, New York, NY 10027 USA

³Department of Physics, University of California, San Diego, La Jolla, CA 92093 USA

⁴National High Magnetic Field Laboratory, Florida State University, Tallahassee, FL, 32306 USA

⁵Department of Physics and Astronomy, McMaster University, Hamilton, ON L8S 4M1, Canada and

⁶Institute of Physics, Chinese Academy of Sciences, Beijing 100190, China

(Dated: October 28, 2014)

A quantum critical point (QCP) occurs upon chemical doping of the weak itinerant ferromagnet $\text{Sc}_{3.1}\text{In}$. Remarkable for a system with no local moments, the QCP is accompanied by non-Fermi liquid (NFL) behavior, manifested in the logarithmic divergence of the specific heat both in the ferro- and the paramagnetic states. $\text{Sc}_{3.1}\text{In}$ displays critical scaling and NFL behavior in the ferromagnetic state, akin to what had been observed only in f -electron, local moment systems. With doping, critical scaling is observed close to the QCP, as the critical exponents δ , γ and β have weak composition dependence, with δ nearly twice, and β almost half of their respective mean-field values. The unusually large paramagnetic moment $\mu_{PM} \sim 1.3\mu_B/\text{F.U.}$ is nearly composition-independent. Evidence for strong spin fluctuations, accompanying the QCP at $x_c = 0.035 \pm 0.005$, may be ascribed to the reduced dimensionality of $\text{Sc}_{3.1}\text{In}$, associated with the nearly one-dimensional Sc-In chains.

INTRODUCTION

Quantum critical points (QCPs) are ubiquitous features in the phase diagrams of strongly correlated electron systems, ranging from high temperature oxide superconductors [1–3] and low-dimensional compounds [4–6], to itinerant magnets (IMs) [7–10] and heavy fermions (HFs) [11–16]. Often, non-Fermi liquid (NFL) behavior [17–21], and critical scaling [22] accompany the QCP, and such novel phenomena have been extensively studied in HFs. However, much less is currently understood about itinerant electron magnets and their quantum critical behavior, particularly due to the limited number of existent IMs. Of these, itinerant *ferromagnets* (IFMs) are particularly appealing, since theoretical predictions suggest that the proximity to a ferromagnetic instability precludes the occurrence of a quantum phase transition (QPT). The QCPs recently observed in two substantively different systems, the IFM ZrZn_2 [7] and the HF ferromagnet URh_2Si_2 [23], are at odds with this prediction. Furthermore, NFL behavior is associated with the quantum phase transition induced by doping in the latter compound, but not the former, reemphasizing the imperious need for a unified picture of quantum criticality and NFL behavior in IFM systems. This study of the doping-induced NFL state close to the QCP in the IFM $\text{Sc}_{3.1}\text{In}$ provides a first connection between the two previously known ferromagnetic QCP systems, a precursor of such a unified theory.

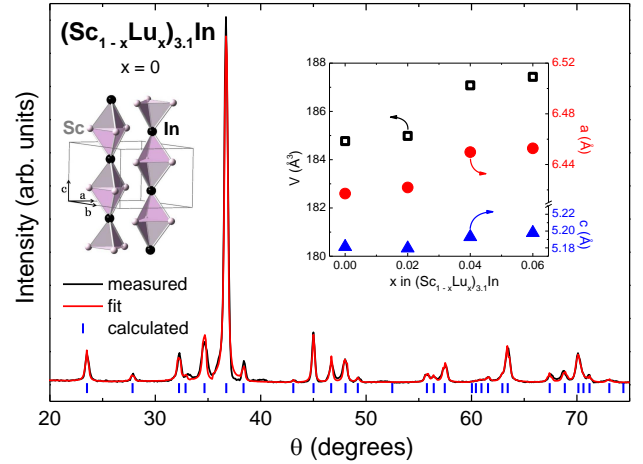


FIG. 1: Measured X-ray diffraction pattern for $(\text{Sc}_{1-x}\text{Lu}_x)_{3.1}\text{In}$ (black line) where $x = 0$, with calculated peak positions marked by blue vertical lines, based on space group $P6_3/mmc$ and lattice parameters $a = 6.42$ Å and $c = 5.18$ Å. The crystal structure of $\text{Sc}_{3.1}\text{In}$ (left inset) exhibits quasi-1D chains of Sc-In. Right inset: evolution of lattice parameters a and c and the unit cell volume V with composition x .

Lu doping in $\text{Sc}_{3.1}\text{In}$ represents the first report of NFL behavior associated with a QPT in this IFM. The critical composition x_c in $(\text{Sc}_{1-x}\text{Lu}_x)_{3.1}\text{In}$ is very small, close to 0.035. The critical scaling close to the QCP is remarkable by comparison to ZrZn_2 or URu_2Si_2 : while $\text{Sc}_{3.1}\text{In}$ is similar to the former compound as the only other known FM with no magnetic elements, its critical scaling is not mean-field-like, akin to that in the latter

*Present Address: Laboratory for Muon Spin Spectroscopy, Paul Scherrer Institut, CH-5232 Villigen PSI, Switzerland

system. The reduced dimensionality of $\text{Sc}_{3.1}\text{In}$, associated with quasi-1D Sc-In chains (inset of Fig. 1), provides a plausible justification for the similarities with the two-dimensional URu_2Si_2 , and contrasts with the three-dimensional ZrZn_2 . In URu_2Si_2 the Kondo effect is inherently coupled with the quantum critical behavior, but $\text{Sc}_{3.1}\text{In}$ has no local moments, rendering its magnetism and the QCP even more striking. What makes $\text{Sc}_{3.1}\text{In}$ even more unique is the NFL behavior, a trait so far only present in f -electron systems. It is therefore paramount to probe the existence of the QCP in this IFM system, and properly characterize the NFL behavior, as a precursor for a unified picture of quantum criticality in IFMs. The development of such a unified theory necessitates more IFM systems, which starts with a thorough understanding of the few compounds that are already known.

IFMs lack the complexity associated with the interplay between the local and itinerant character of the electrons observed in HFs [15, 24]. Of the two known IFMs with no magnetic elements, ZrZn_2 and Sc_3In , the latter presents the advantage, from the quantum criticality perspective, of a much lower magnetic ordering temperature $T_C \leq 7.5$ K [25–29] in Sc_3In . This would likely facilitate the suppression of magnetic order towards a QCP, but has proven difficult by the application of pressure [29] or magnetic field [27]. Here we show that the QCP in $\text{Sc}_{3.1}\text{In}$ can indeed be reached by Lu doping, where the dopant ion is comparable in size ($r[\text{Lu}^{3+}] = 0.861$ Å) with the host ion Sc that it substitutes for ($r[\text{Sc}^{3+}] = 0.745$ Å) [30]. This way, the effects of chemical substitution can be deconvoluted from those of chemical pressure, which is important given that pressure was shown to enhance the ordering temperature [29]. The systematic analysis of the magnetization isotherms $M(H)$, temperature-dependent magnetization $M(T)$ at low fields, and $H = 0$ specific heat data, for $0 \leq x \leq 0.10$ indicate that the magnetic ground state is suppressed in $(\text{Sc}_{1-x}\text{Lu}_x)_{3.1}\text{In}$ towards a QCP close to $x_c \approx 0.035$. Remarkably, the logarithmic divergence of the specific heat close to x_c evidences NFL behavior in both the ferromagnetic and the paramagnetic state. Additionally, the reduced dimensionality, associated with quasi-1D Sc-In chains, may be linked to the NFL behavior and the non-mean-field critical scaling, similar to that in the more 2D FM, albeit with substantively different critical exponents.

EXPERIMENTAL METHODS

The hexagonal $\text{Sc}_{3.1}\text{In}$ compound has a Ni_3Sn -type structure, with space group $\text{P6}_3/\text{mmc}$ and lattice parameters $a = 6.42$ Å and $c = 5.18$ Å [31]. The reported crystal structure for Sc_3In is shown in the left inset of Fig. 1. Highlighted are the Sc-In bipyramids which form nearly one dimensional chains along the hexagonal c axis. Band structure calculations [32] indicate that this crystal

structure also renders the electronic configuration nearly one dimensional. These observations will be discussed in the context of the dimensionality of other IFM systems close to quantum criticality.

It had already been established [25] that Sc_3In forms non-stoichiometrically around the ionic ratio $\text{Sc}:\text{In} = 3:1$. In the current study, we have determined that the optimal composition, which yielded the highest Curie temperature T_C and paramagnetic moment μ_{PM} , was $\text{Sc}:\text{In} = 3.1:1$. Polycrystalline samples of $(\text{Sc}_{1-x}\text{Lu}_x)_{3.1}\text{In}$ ($0 \leq x \leq 0.10$) were prepared by arc-melting Sc (Ames Laboratory, 99.999%), Lu (Ames Laboratory, 99.999%) and In (Alfa Aesar, 99.9995%), with mass losses no more than 0.5%. The arc-melted buttons were subsequently wrapped in Ta foil, sealed in quartz tubes under partial Ar atmosphere, and annealed over two weeks at temperatures between 700°C and 800°C.

Both annealed and non-annealed samples exhibit extreme hardness, comparable to that of high carbon steels [33], which made it very difficult to perform powder x-ray diffraction measurements. However, it was feasible to x-ray a polished surface of the arc-melted buttons. The arc-melted samples with radius of about 3 mm were cut, and the flat surface was scanned for 12 hours in a Rigaku D/Max diffractometer with $\text{CuK}\alpha$ radiation and a graphite monochromator. An example of a diffraction pattern is shown in Fig. 1 for $(\text{Sc}_{1-x}\text{Lu}_x)_{3.1}\text{In}$ with $x = 0$. All observed peaks can be indexed with the space group $\text{P6}_3/\text{mmc}$. As shown in the right inset of Fig. 1, both a (right axis, circles) and c (right axis, triangles) lattice parameters, along with the unit cell volume V (left axis, squares) for $(\text{Sc}_{1-x}\text{Lu}_x)_{3.1}\text{In}$ for $0 \leq x \leq 0.10$, increase nearly linearly with x .

DC magnetization measurements on the annealed samples were performed in a Quantum Design (QD) Magnetic Property Measurement System for temperatures between 1.8 K and 300 K, and for applied magnetic fields up to 5.5 T. Specific heat was measured from 0.4 K to 20 K in a QD Physical Property Measurement System.

Measurements of AC magnetic susceptibility were performed in a ^4He dewar down to ~ 1.17 K, with temperatures below 4.2 K achieved by pumping on the ^4He bath with a Stokes pump. The AC magnetic susceptibility coils were positioned in the thermal gradient above the ^4He bath by manually adjusting the vertical position of the probe. An AC current was driven on the primary coils with a frequency of 15.9 Hz using a Linear Research LR700 AC resistance bridge, which produces an AC magnetic field with magnitude of ~ 0.3 Oe. This bridge was also used to measure the in- and out-of-phase components of the signal induced in the secondary pickup coils. The secondary coils are balanced by counter-winding the wire to cancel background signals induced by the oscillating AC magnetic field. A small offset in the measured signal due to minor imbalances in the home-built AC susceptibility coils was subtracted from the data. The data were

then scaled so that their arbitrary units are proportional to emu/mol.

Muon Spin Relaxation (μ SR) measurements were performed at TRIUMF using a He gas flow cryostat at the M20 beamline for $\text{Sc}_{3.1}\text{In}$ and another spectrometer with dilution cryostat at the M15 beamline for $x = 0.01$ and $x = 0.025$ ($\text{Sc}_{1-x}\text{Lu}_x$) $_{3.1}\text{In}$ samples. Details of the μ SR technique can be found elsewhere [34–38].

RESULTS AND ANALYSIS

Temperature-Dependent Magnetization Measurements

For weak IFMs, the low-field susceptibility is expected to follow a T^{-1} behavior [39]:

$$\frac{\chi_0}{\chi(T)} = 1 - \alpha + \lambda(T), \quad (1)$$

where the coefficient λ encompasses the dependence on the local amplitude of spin fluctuations and is linear in temperature $\lambda \sim T/T_C^*$, and $\alpha = I\rho(E_F)$, where I is the coupling constant and $\rho(E_F)$ is the density of states at the Fermi level. When $T^* \gg T_C^*$, $\alpha \sim (T/T^*)^2$ usually has only a weak T^2 dependence. However, the magnetic susceptibility $\chi(T)$ in $\text{Sc}_{3.1}\text{In}$ follows a modified Curie-Weiss-like law:

$$\chi(T) = \frac{C}{T^*} + \frac{C}{(T - T_C^*)}, \quad (2)$$

as illustrated in Fig. 2(a). Such a temperature dependence can possibly be understood when considering strong spin fluctuations, associated with the nearly one-dimensional Fermi surface of Sc_3In [32]: if $T^* > T_C^*$ (but *not* $\gg T_C^*$), then the temperature dependence of α is not negligible compared to that of λ . In weak IFMs, the Curie-Weiss-like temperature T_C^* , determined from linear fits of the inverse susceptibility after the temperature independent term C/T^* was subtracted, coincides with the Curie temperature T_C . As shown below, this is not the case in ($\text{Sc}_{1-x}\text{Lu}_x$) $_{3.1}\text{In}$, even though T_C and T_C^* are both continuously suppressed to 0 K with x .

A local minimum in the derivative dM/dT (Fig. 2(b), left axis) corresponds to the Curie temperature T_C in $\text{Sc}_{3.1}\text{In}$. Moreover, the specific heat data for $x = 0$, plotted as C_p/T (right axis, Fig. 2(b)), also displays a broad maximum at T_C . This is remarkable, given that such transitions are often difficult to identify in the field-independent properties of IFMs, even in single crystalline samples [23]. In $\text{Sc}_{3.1}\text{In}$, the susceptibility derivatives and specific heat data provide evidence that the ferromagnetic ordering occurs below $T_C \sim 4.5$ K, as also demonstrated by the field-dependent data shown below. The

different measurements consistently indicate that T_C is significantly lower than the older estimates from Arrott isotherms alone [26, 28, 29], when Sc_3In was erroneously assumed to be a mean-field ferromagnet.

In ($\text{Sc}_{1-x}\text{Lu}_x$) $_{3.1}\text{In}$, T_C is continuously suppressed by Lu doping above $x = 0.02$ to values below those accessible by the QD MPMS system. Further data below $T = 2$ K was collected from ^4He AC susceptibility measurements shown in Fig. 2(c). Lack of data around the 4.2 K ^4He transition precludes a T_C estimate for $x = 0$ and $x = 0.005$, when the transition falls close to this temperature interval. However, for all other compositions up to $x = 0.04$, the peak corresponding to T_C (illustrated by the solid line fit in Fig. 2(c)) is continuously reduced to temperatures below $T = 1.17$ K, as shown in Fig. 2(c). This agrees with the critical composition $x_c = 0.035 \pm 0.005$, as determined from the analysis below.

Arrott and Arrott-Noakes Analysis

Strong spin fluctuations in $\text{Sc}_{3.1}\text{In}$ result in deviations from linearity in the inverse susceptibility around T_C^* which precludes the accurate determination of the Curie temperature T_C from the $\chi(T)$ data. Alternatively, Arrott isotherms M^2 vs. H/M [40] had previously been employed to determine T_C in Sc_3In . Existing reports give this value to be less than 7.5 K [25–29]. If the Arrott plot technique were used for $\text{Sc}_{3.1}\text{In}$ (Fig. 3(a)), it would appear that ferromagnetic order occurred close to 9.75 K. This implies that the Sc-In ratio used for the current study is closest to the optimal one [25], compared to all previous reports. However, the Arrott isotherms deviate strongly from linearity at high H values [26, 28, 29]. This is a compelling indication that the mean-field theory cannot accurately describe the weak ferromagnetism in $\text{Sc}_{3.1}\text{In}$, in contrast with, for example, ZrZn_2 [7]. The more generalized Arrott and Noakes method[41] was successfully employed to characterize the critical scaling in the HF ferromagnet URu_2Si_2 doped by Re [23]. In the current work, this generalized critical scaling is applied to a different type of QCP, in the weak IFM $\text{Sc}_{3.1}\text{In}$ which has no local moment elements. It would appear that the NFL behavior results from the non-mean field character of the magnetism in these IFMs.

The Arrott-Noakes scaling represents a generalization of the mean-field scaling of the magnetization M , magnetic field H and the reduced temperature $t = (T/T_C - 1)$:

$$M \propto t^\beta \text{ for } t < 0 \quad (3)$$

$$M \propto H^{1/\delta} \text{ at } t = 0 \quad (4)$$

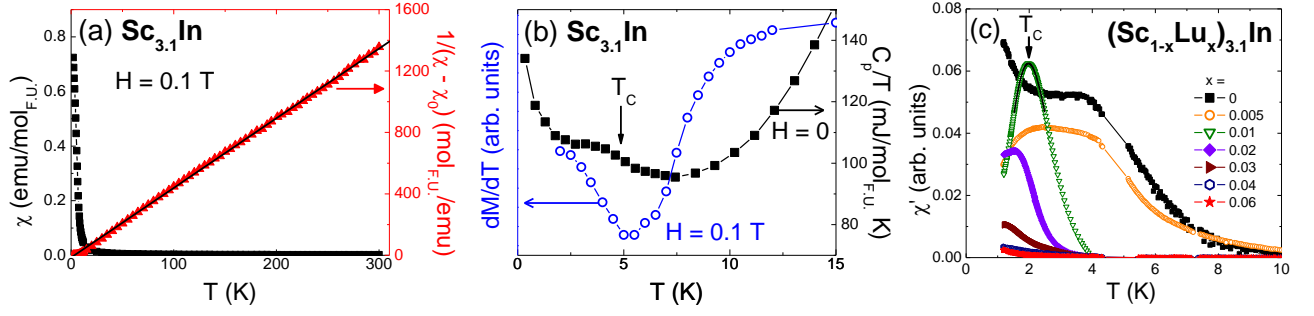


FIG. 2: (a) $\text{Sc}_{3.1}\text{In}$ susceptibility (left) and inverse susceptibility $1/(\chi - \chi_0)$ (right) for $H = 0.1$ T, where $\chi_0 = C/T^*$ (see text). (b) The magnetization derivative dM/dT (left) and specific heat C_p/T (right) for $\text{Sc}_{3.1}\text{In}$ with the vertical arrow marking the Curie temperature T_C . (c) $(\text{Sc}_{1-x}\text{Lu}_x)_{3.1}\text{In}$ AC susceptibility $\chi'(T)$. The Curie temperature T_C is estimated from the peak position (solid line), indicated by the vertical arrow.

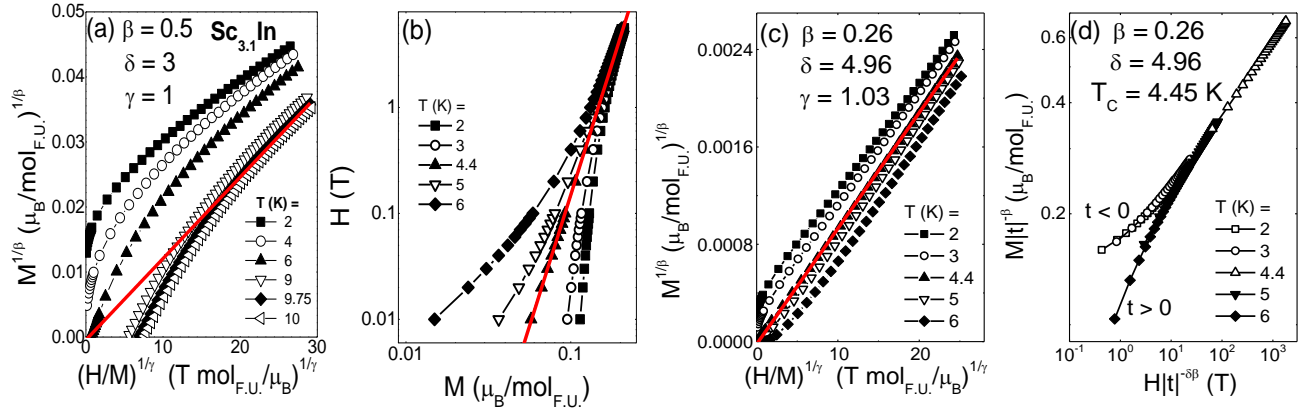


FIG. 3: $M^{1/\beta}$ vs. $(H/M)^{1/\gamma}$ isotherms for $\text{Sc}_{3.1}\text{In}$ with (a) mean field exponents $\beta = \beta_{MF} = 0.5$ and $\gamma = \gamma_{MF} = 1$, $T_C = 9.75$ K (solid line) and (c) non-mean-field exponents $\beta = 0.26$ and $\gamma = 1.03$, $T_C = 4.45$ K (solid line). (b) Log-log plot of $\text{Sc}_{3.1}\text{In}$ $M(H)$ isotherms, with the straight line representing the fit for the critical isotherm. (d) Arrott-Noakes scaling plots $M|t|^{-\beta}$ vs. $H|t|^{-\delta\beta}$. The scaled $M(H)$ data collapses onto two diverging branches, one below T_C ($t < 0$, open symbols) and one above T_C ($t > 0$, full symbols).

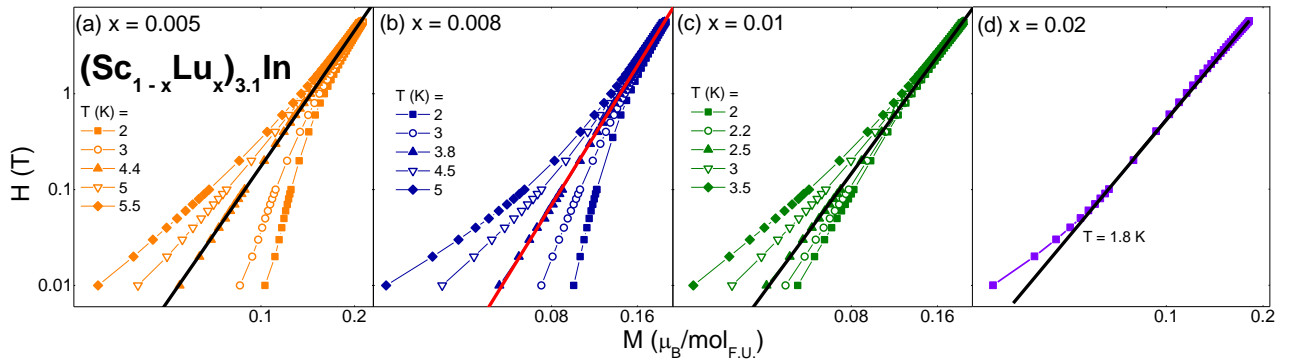


FIG. 4: Log-log $(\text{Sc}_{1-x}\text{Lu}_x)_{3.1}\text{In}$ $M(H)$ isotherms for (a) $x = 0.005$, (b) $x = 0.008$ and (c) $x = 0.01$ with linear fits (solid lines) at the critical ($T = T_C$) isotherm. (d) Log-log $M(H)$ curve for $x = 0.02$ and $T = 1.8$ K, with a linear fit above $H = 0.05$ T.

$$\chi \propto t^{-\gamma} \text{ for } t > 0 \quad (5)$$

This yields generalized critical exponents β , δ and γ with the constraint that $1 + \gamma/\beta - \delta = 0$. In the case of $(\text{Sc}_{1-x}\text{Lu}_x)_{3.1}\text{In}$, the Curie temperature T_C and exponent δ are first determined from log-log $M(H)$ plots for each composition, as shown in Fig. 3(b) for $x = 0$ and in Fig. 4(a-c) for $x = 0.005, 0.008$, and $x = 0.01$. At T_C , critical scaling requires that the isotherm be linear, with a slope equal to the critical exponent δ . The $T = 1.8$ K isotherm for $x = 0.02$ is nearly linear all the way down to $H = 0$ T (Fig. 4(d)), indicating that T_C for $x = 0.02$ is finite and smaller than 1.8 K. For all other FM compositions (Fig. 4(a-c)), non-linear isotherms occur within 20% of T_C . Therefore, in the absence of $M(H)$ measurements below 1.8 K, the nearly linear log-log $M(H; 1.8 \text{ K})$ isotherm for $x = 0.02$ is a good indication that the T_C value estimate for this composition is within 20% of T_C , which yields $T_C(x = 0.02) = 1.5 \pm 0.3$ K. This value agrees well with the AC susceptibility estimate, where $T_C = 1.62$ K.

Next, the critical exponents β and γ are determined from the expected linear dependence of $M^{1/\beta}$ vs. $(H/M)^{1/\gamma}$. A subset of the resulting isotherms is shown in Figs. 3(c) ($x = 0$) and 5(a-c) ($x = 0.005, 0.008$ and 0.01). The extrapolations of the linearized isotherms in the ferromagnetic state yield the spontaneous magnetization M_0 from the vertical axes intercepts. As expected, M_0 scales with $|t|^\beta$, as shown in Fig. 6 for $(\text{Sc}_{1-x}\text{Lu}_x)_{3.1}\text{In}$ where $0 \leq x \leq 0.02$. In contrast with $\text{URu}_{2-x}\text{Re}_x\text{Si}_2$ [23], M_0 for $(\text{Sc}_{1-x}\text{Lu}_x)_{3.1}\text{In}$ (Fig. 6) grows faster in the ordered state, as the critical exponent β for the former, $\beta = 0.26 \pm 0.05$, is less than half of the respective value in the latter system [23]. However, the β values in $(\text{Sc}_{1-x}\text{Lu}_x)_{3.1}\text{In}$ are unusually small, which implies that the ordered moment in this weak IFM is more readily destabilized by fluctuations close to T_C . This might indicate a fragile magnetism in a nearly 1D electron system [32], which doping and the attendant disorder immediately suppress to 0 K.

The Arrott-Noakes critical exponents δ (triangles), γ (squares) and β (circles), scaled by their mean-field (MF) values, are presented in Fig. 7 as a function of composition. Most strikingly, δ is nearly twice as large as its mean-field value δ_{MF} , while β is nearly half of β_{MF} , leaving γ nearly identical to its mean-field value γ_{MF} . δ is a measure of the curvature of $M(H)$ at T_C , with larger values signaling faster saturation. A comparison between $(\text{Sc}_{1-x}\text{Lu}_x)_{3.1}\text{In}$ and $\text{URu}_{2-x}\text{Re}_x\text{Si}_2$ [23] shows that larger δ values for the former compound are also associated with a larger relative magnetization $M(5.5 \text{ T}; 1.8 \text{ K}) \approx 0.2 \mu_B$. This value at $t = 0.6$ is nearly 15% of the paramagnetic moment $\mu_{PM} \approx 1.3 \mu_B$ for the composition $x = 0$ with maximum T_C . The corresponding value for $\text{URu}_{2-x}\text{Re}_x\text{Si}_2$ is $M(5.5 \text{ T}; 1.8 \text{ K})/\mu_{PM} \approx$

$(0.4 \mu_B)/(3.8 \mu_B) \approx 10\%$ (for which $T_{C,max} = 27$ K is obtained for $x = 0.6$), nearly one third less at a comparable relative temperature t (Fig. 1, bottom panel, in Ref. [24]).

The scaling collapse of $M|t|^{-\beta}$ vs. $H|t|^{-\delta\beta}$, shown in Figs. 3(d) and 8(a-c), exemplifies how the $M|t|^{-\beta}$ vs. $H|t|^{-\delta\beta}$ curves collapse onto two diverging branches, for $t < 0$ (open symbols) and $t > 0$ (full symbols). This collapse is similar to that observed for the HF $\text{URu}_{2-x}\text{Re}_x\text{Si}_2$ [23], which is remarkable, given the lack of formal local moments in the constituent elements of $(\text{Sc}_{1-x}\text{Lu}_x)_{3.1}\text{In}$.

Non-Fermi Liquid Behavior

An independent and compelling evidence for the QCP in the doped $\text{Sc}_{3.1}\text{In}$ system is the NFL behavior below $x = 0.04$. The signature of NFL behavior is the logarithmic divergence of the specific heat C_p/T (Fig. 9(a)), which occurs over a decade in temperature. This divergence of the specific heat, shown in Fig. 9(a), may have two possible origins: NFL behavior or Schottky anomaly. For a Schottky anomaly, a low- T peak in the specific heat would move up in temperature with increasing H . However, the decrease of the low temperature C_p/T with increasing H (Fig. 9(b)) invalidates the Schottky anomaly scenario and not surprisingly, since this would be associated with low-lying energy states (not the case for a system with no formal local moments). The NFL scenario is therefore more plausible in $(\text{Sc}_{1-x}\text{Lu}_x)_{3.1}\text{In}$ for $0 \leq x \leq 0.04$. More interestingly, the NFL behavior coexists with the ferromagnetic state. This coexistence has been explained based on magnetic cluster formation as a result of competition between Ruderman-Kittel-Kasuya-Yosida (RKKY) coupling and Kondo effect [42, 43]. However, this is the *first* observation of NFL behavior within the ferromagnetic state in a weak IFM. The implication is that a new model would be required to describe the ground state in $\text{Sc}_{3.1}\text{In}$, or that the Griffiths-McCoy model [44] may still be appropriate if evidence for Kondo effect emerged for this compound.

Muon Spin Relaxation Measurements

The small saturation moments of itinerant systems preclude neutron diffraction investigations, similar to the case of ZrZn_2 [45]. On the contrary, the muon spin relaxation (μSR) technique is extremely sensitive to local magnetic fields and has been used to investigate multiple itinerant systems [46–50]. Figure 10 shows the time spectra observed in zero field (ZF) and longitudinal field (LF) at the lowest temperature. The fast relaxation in the early time region in ZF is eliminated by the decoupling effect in LF, which indicates that the observed relaxation

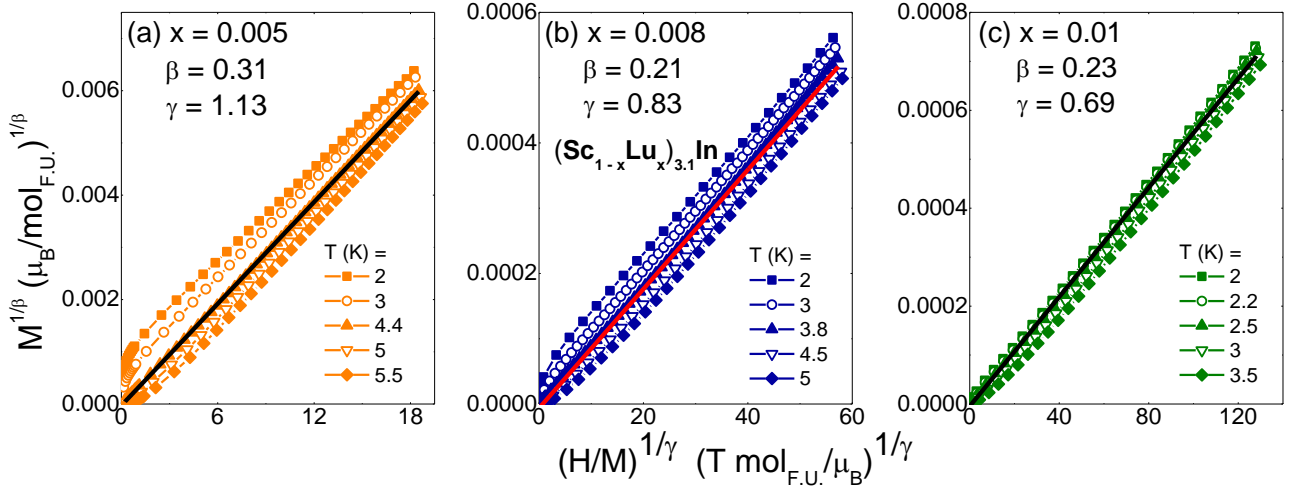


FIG. 5: $(\text{Sc}_{1-x}\text{Lu}_x)_{3.1}\text{In}$ Arrott-Noakes $M^{1/\beta}$ vs. $(H/M)^{1/\gamma}$ isotherms for (a) $x = 0.005$, (b) $x = 0.008$, and (c) $x = 0.01$ with linear fits (solid lines) at T_C .

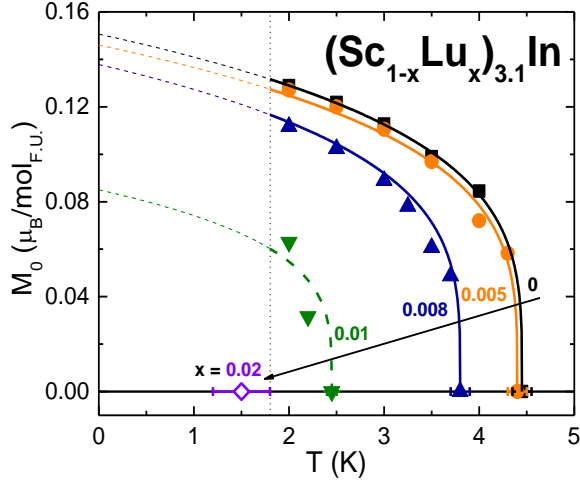


FIG. 6: Spontaneous magnetization $M_0(T)$ for $(\text{Sc}_{1-x}\text{Lu}_x)_{3.1}\text{In}$ where $0 \leq x \leq 0.02$.

is due to a static field, generated by the static magnetic order in both the undoped and doped systems. For the ZF $\text{Sc}_{3.1}\text{In}$ spectrum, two precession frequencies at low temperatures can be seen, as shown in Fig. 11(a). The ZF time spectra were analyzed by assuming a functional form of:

$$G(t) = [A_1 \cos(2\pi\nu_1 t) e^{(-\Lambda_1^2 \frac{t^2}{2})} + A_2 \cos(2\pi\nu_2 t) e^{(-\Lambda_2^2 \frac{t^2}{2})} + (A_{1Z} + A_{2Z}) e^{(-\frac{t}{T_1})}] V_M + \frac{(1 - V_M)[G_{KT}(t, \Delta_{KT1}) + G_{KT}(t, \Delta_{KT2})]}{2} \quad (6)$$

where $G_{KT}(t)$ is the Kubo-Toyabe function [51] for random nuclear dipolar fields, and A_{1Z} and A_{2Z} are assumed to be a half of A_1 and A_2 , respectively, as expected for polycrystalline specimens. A very good fit was obtained by assuming $A_1 = A_2$, presumably due to two magnetically-nonequivalent muon sites populated

with equal probabilities. For the longitudinal relaxation rate $1/T_1$, two values for the two different sites could not be resolved. So, one value of T_1 was used in the fit. The temperature dependence of the two frequencies ν_1 and ν_2 is shown in Fig. 11(a). The volume fraction V_M of the magnetically ordered region, shown in Fig. 11(b),

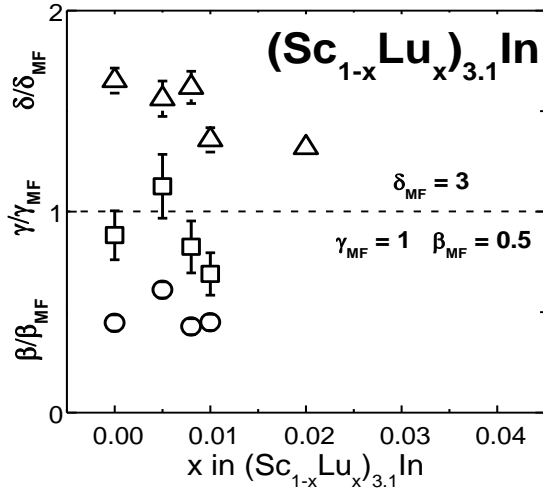


FIG. 7: The critical exponents scaled by their mean-field values δ/δ_{MF} (triangles), γ/γ_{MF} (squares) and β/β_{MF} (circles) as a function of composition x .

was determined from the amplitudes of the precession signals. The volume fraction V_M decreases gradually with increasing temperature, indicating co-existence of volumes (or regions) with and without static magnetic order. Although the precession signal disappears around $T = 5.5$ K, a small V_M remains above this temperature up to $T \approx 8$ K. This is due to a non-precessing but relaxing signal with a small amplitude, caused by static random fields from the electron system remaining in a small volume fraction.

The Lu-doped samples show relaxing signal without precession at low temperatures, indicating a more random internal field, as compared with the undoped $\text{Sc}_{3.1}\text{In}$. In order to reproduce the observed line shape, the ZF time spectra of the Lu-doped samples have been analyzed by assuming the following functional form:

$$G(t) = A_1(1 - p\sigma^2)e^{-\frac{1}{2}\sigma^2 t^2} + \frac{A_1}{2}e^{(-\frac{t}{T_1})} + A_{bg} \quad (7)$$

where the first term represents the transverse relaxation, the second term is the longitudinal $1/T_1$ component, and the third term is a background signal from the sample holder. From independent measurements in weak transverse field at low temperatures, the values of the non-relaxing background signal from a silver sample holder A_{bg} were estimated to be 0.36 and 0.55 for $x = 0.01$ and 0.025 samples, respectively. These values are consistent with the known background level from the cryostat and sample holder, and a rather small sample size. It is, however, not possible to eliminate the possibility that signal from a small paramagnetic volume in the specimen, persisting to $T = 0$ K, is included in the background signal. Due to difficulty in separating the effects of slow relaxation and partial volume fraction, the amplitude A_1 was

fixed to be temperature-independent, allowing to extract the relaxation rate σ . A phenomenological "dip" parameter p ($p = 1$) for the Kubo-Toyabe function was introduced, while smaller p values would fit line shapes with a shallower dip, which are often observed in real materials, including the present case of Lu-doped systems. Although the fit is not perfect, as shown by the lines in Fig. 10, the functional form of Eq. 7 was used to compare the relaxation rates in different specimens without introducing additional free parameters. Fig. 12(a) shows the temperature dependence of σ in the two Lu-doped specimens. To compare the relaxation rates σ with the static field measured in undoped $\text{Sc}_{3.1}\text{In}$, the spatially averaged value of the static local field was determined as:

$$H_{av} = V_M \frac{A_1\nu_1 + A_2\nu_2}{A_1 + A_2} + \frac{(1 - V_M)(\Delta_{KT1} + \Delta_{KT2})}{2\gamma_\mu} \quad (8)$$

where γ_μ represents the gyromagnetic ratio of a positive muon and Δ_{KT} are the widths of the Kubo-Toyabe function for nuclear dipolar fields. We plot H_{av} in Fig. 12(a) with the relaxation rate (left axis) and the average field (right axis), scaled with γ_μ . Since the static internal field is expected to be proportional to the local static spin polarization, Fig. 12(a) demonstrates the development of the spatially-averaged magnetic order parameter which can be compared to the spontaneous magnetization M_0 , shown in Fig. 6.

Measurements of the spin-lattice relaxation rate $1/T_1$ were performed in an applied LF. Figure 12(b) shows the temperature dependence of $1/T_1$ for $(\text{Sc}_{1-x}\text{Lu}_x)_{3.1}\text{In}$ with $x = 0, 0.01, 0.025$. There is no divergent behavior in $\text{Sc}_{3.1}\text{In}$, while the Lu-doped samples exhibit a peak in $1/T_1$ at the ordering temperature. In either case, the absolute values of $1/T_1$ are less than $0.1/\mu\text{s}$, which implies that the relaxation rate measured in zero field (Fig. 12(a)) is predominantly due to a static field, even at temperatures very close to the ordering temperature. In Fig. 12(a), a finite relaxation rate/average field persists up to high temperatures for all the three systems. This is attributed to the nuclear dipolar field, as Sc has a very large nuclear moment.

The absence of dynamic critical behavior and the gradual change of the volume fraction V_M , observed in undoped $\text{Sc}_{3.1}\text{In}$, indicates a first-order transition at the magnetic order. It is interesting to note that a weak "second order" feature is observed for Lu-doped samples. However, further experimental data are needed given the fact that the order parameter (Fig. 12(a)) exhibits a non-linear dependence on the Curie temperature T_C , suggesting a remaining effect of first-order quantum evolution. Additionally, the difficulty in separating the effects of moment sizes and volume fraction at very small relaxation rates, as well as the uncertainty in estimating

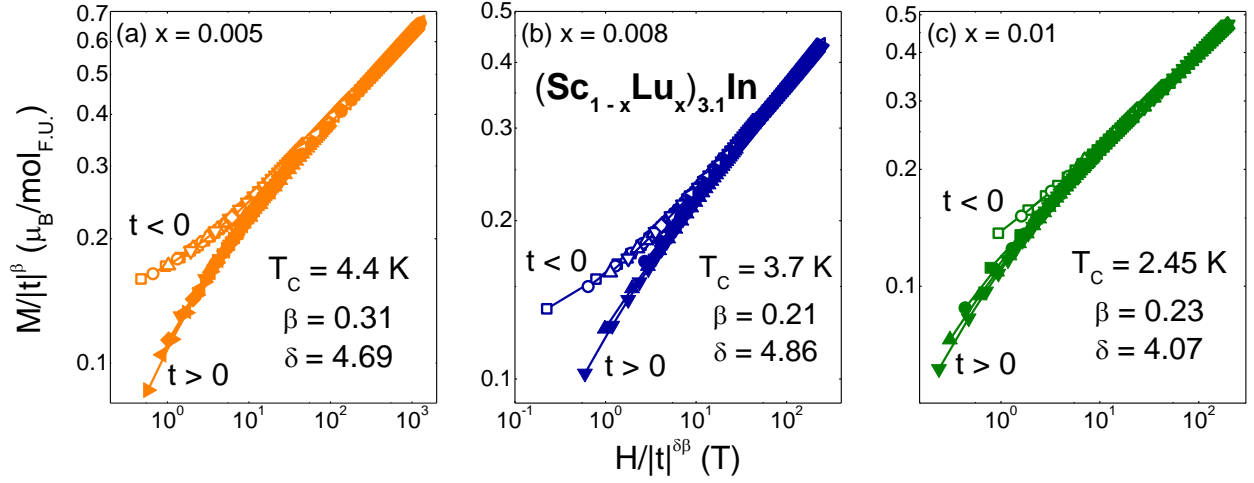


FIG. 8: Scaling plots $M|t|^{-\beta}$ vs. $H/|t|^{\delta\beta}$ for (a) $x = 0.005$, (b) $x = 0.08$ and (c) $x = 0.01$ in $(\text{Sc}_{1-x}\text{Lu}_x)_{3.1}\text{In}$.

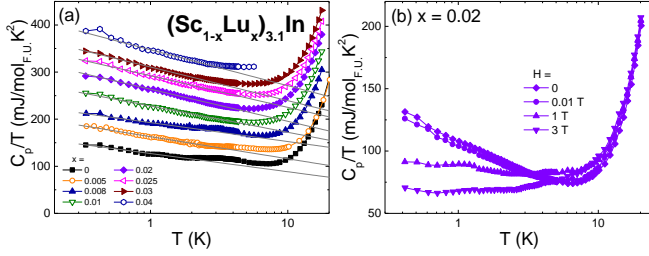


FIG. 9: (a) Semi-log plot of the specific heat C_p/T (symbols) and the linear fits (lines) at low temperatures. The data for $x > 0$ are shifted vertically for clarity by 30 mJ/mol_{F.U.} K². (b) Specific heat for $(\text{Sc}_{0.98}\text{Lu}_{0.02})_{3.1}\text{In}$ in various magnetic fields: $H = 0, 0.01, 1$ and 3 T.

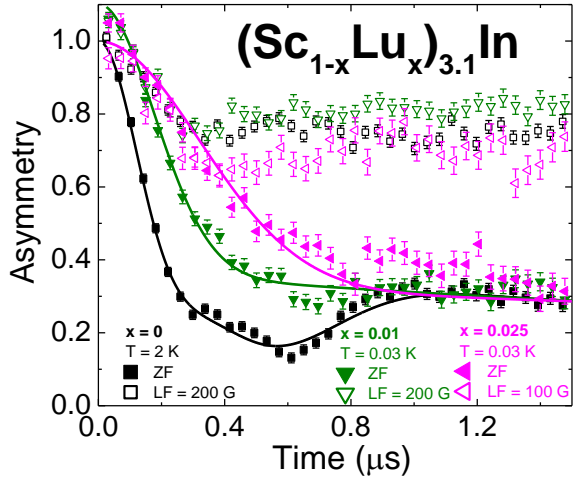


FIG. 10: Time spectra of ZF and LF μSR of $(\text{Sc}_{1-x}\text{Lu}_x)_{3.1}\text{In}$ where $x = 0$ (squares), 0.01 (downward-facing triangles) and 0.025 (leftward-facing triangles). The background sample holder contribution in the two Lu-doped samples was subtracted. The solid lines represent fits to Eqs. 6 and 7.

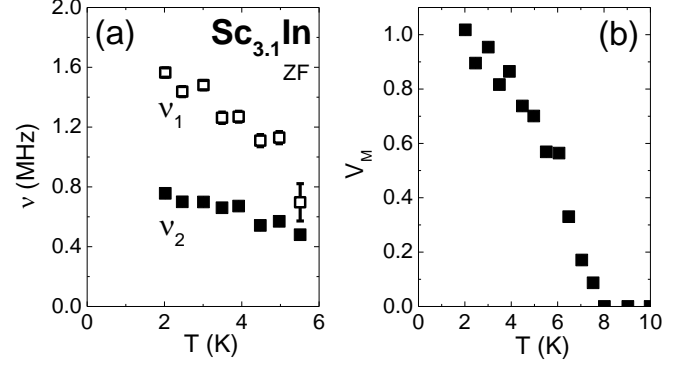


FIG. 11: (a) The muon spin precession frequencies ν_1 (full squares) and ν_2 (open squares), and (b) the volume fraction V_M of the magnetically ordered regions, obtained from ZF μSR of $\text{Sc}_{3.1}\text{In}$

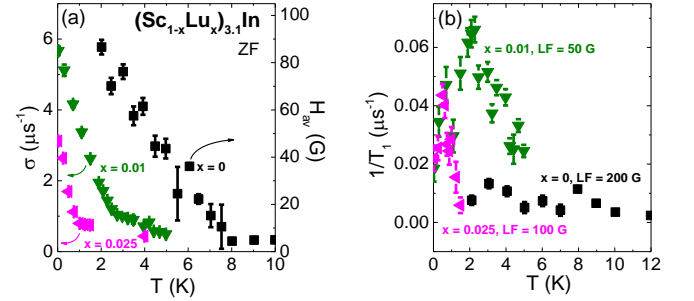


FIG. 12: (a) Muon spin relaxation rate σ for $x = 0.01$ (downward-facing triangles) and $x = 0.025$ (leftward-facing triangles) for $(\text{Sc}_{1-x}\text{Lu}_x)_{3.1}\text{In}$ (left axis) along with the average static internal field H_{av} for $x = 0$ (right axis), obtained from the fits of ZF μSR measurements. The vertical axes are scaled with γ_μ , the gyromagnetic ratio of a positive muon. (b) The longitudinal relaxation rate $1/T_1$, obtained from the LF μSR measurements.

background level, prevent reliable determination of V_M for the Lu-doped samples.

DISCUSSION

The paramagnetic moment μ_{PM} (diamonds, Fig. 13(a)), determined from the Curie-Weiss-like law, is nearly composition-independent $\mu_{PM} \sim 1.3\mu_B/FU$. Moreover, the Weiss-like temperature T_C^* decreases nearly linearly with x for $x \leq 0.10$, after an initial jump between $x = 0$ and 0.005 (squares, Fig. 13(a)). Considering that Curie-Weiss-like behavior in the itinerant scenario arises from the temperature-dependence of the amplitude of spin fluctuations [39], this sudden increase in the corresponding T_C^* signals enhanced spin fluctuations due to the disorder brought on by Lu doping. Between $x = 0.02$ and $x = 0.04$, T_C^* changes sign in a continuous manner, suggesting the presence of a (second order) doping-induced QCP in this composition range near $x_c = 0.035 \pm 0.005$. Moreover, T_C determined either from $\chi'(T)$ or $M(H)$ data (Figs. 2(c)-5) moves down in temperature below 1.17 K for the doping amounts above 0.03, indicating that the QCP is close to this composition.

The determination of the critical composition x_c at the QCP requires consistency between the $M(T)$ and $\chi'(T)$ data, the critical scaling analysis of the $M(H)$ measurements as well as the μ SR results. Indeed, the critical composition $x_c = 0.035 \pm 0.005$ is determined from (i) the T_C (circles and triangles) and T_C^* (squares) values (Fig. 13(b)) approaching 0 K at the QCP and (ii) the critical scaling rendering the Arrott-Noakes plots $M^{1/\beta}$ vs. $(H/M)^{1/\gamma}$ as parallel isotherms, equally spaced in t (Figs. 3(c) and 5(a-c)). Moreover, the μ SR results confirm the development of static magnetic order with a nearly full volume fraction at low temperatures, and diminishing moment size as a function of decreasing ordering temperature. Moreover, the continuous variation of T_C^* and T_C with x and the μ SR evidence for a second order phase transition in the Lu doped samples are also evidence for the QPT induced by Lu doping.

Doping in $\text{Sc}_{3.1}\text{In}$ reveals intriguing traits associated with quantum criticality in general, and with weak IFM systems in particular: the paramagnetic moment μ_{PM} is surprisingly large in $(\text{Sc}_{1-x}\text{Lu}_x)_{3.1}\text{In}$, and nearly independent of x , even as the system goes through the QPT at $x_c = 0.035 \pm 0.005$. Not surprisingly then, the critical exponent β is unchanged through the ferromagnetic state, although its value $\beta = 0.26 \pm 0.05$ is smaller than that in any other known quantum critical system. The minute critical composition and small β value, together with the jump in T_C^* as $x > 0$ (Fig. 13(b), squares) point to a weak IFM ground state, easily perturbed by doping. This may seem unusual in light of the stark differences between $\text{Sc}_{3.1}\text{In}$ and the related IFM

system ZrZn_2 [7], well described by mean-field theory, or the similarities with the extraordinary critical scaling in the HF FM $\text{URu}_{2-x}\text{Re}_x\text{Si}_2$ [23], close to these systems' respective doping-induced QCPs. However, these observations may be reconciled from crystallographic and electronic properties considerations: as a nearly 1D structure is formed by bipyramidal Sc-In chains (inset of Fig. 1), the reduced dimensionality in $\text{Sc}_{3.1}\text{In}$ renders it more similar to the layered (2D) URu_2Si_2 compound than the cubic (3D) ZrZn_2 . It appears that the NFL behavior in the ferromagnetic state may also be correlated with the non-mean-field scaling, and, more importantly, that this correlation is independent of the presence of hybridized f -electrons. Consequently, the universality of the quantum critical behavior common to the former two compounds may be ascribed to spin fluctuations, associated with reduced crystallographic dimensionality. More IFM systems are needed to probe this universality. Equally important is the synthesis of single crystals of $\text{Sc}_{3.1}\text{In}$, which would enable further characterization of the implications of dimensionality on the QCP, as well as to probe the potential NFL behavior at the QCP and in the ferromagnetic state. These experiments are currently underway.

ACKNOWLEDGMENTS

We thank L. L. Zhao for help with figure edits, P. C. Canfield for providing some of the rare earth metals, and Q. Si and M. C. Aronson for useful discussions. The work at Rice was supported by NSF DMR 0847681. Measurements of the AC magnetic susceptibility were performed at UCSD with support from the National Science Foundation under Grant No. DMR-1206553. Work at Columbia and TRIUMF (L.L., B.F. and Y. J. U.) is supported by NSF grants DMR-1105961 and OISE-0968226 (PIRE), REIMEI project from JAEA, Japan, and the Friends of Todai Inc. Foundation. Work at IOPCAS was supported by NSF and MOST of China through research projects.

-
- [1] J. Orenstein and A. J. Millis. Advances in the physics of high-temperature superconductivity. *Science*, 288:468, 2000.
 - [2] S. Sachdev. Quantum criticality: competing ground states in low dimensions. *Science*, 288:475, 2000.
 - [3] G. S. Boebinger, Y. Ando, A. Passner, T. Kimura, M. Okuya, J. Shimoyama, K. Kishio, K. Tamasaku, N. Ichikawa, and S. Uchida. Insulator-to-metal crossover in the normal state of $\text{La}_{2-x}\text{Sr}_x\text{CuO}_4$. *Physical Review Letters*, 77:5417, 1996.
 - [4] Y. F. Dai, H. Zhang, S. Y. Zhou, B. Y. Pan, X. Qiu, X. C. Hong, T. Y. Guan, J. K. Dong, Y. Chen, and S. Y. Li.

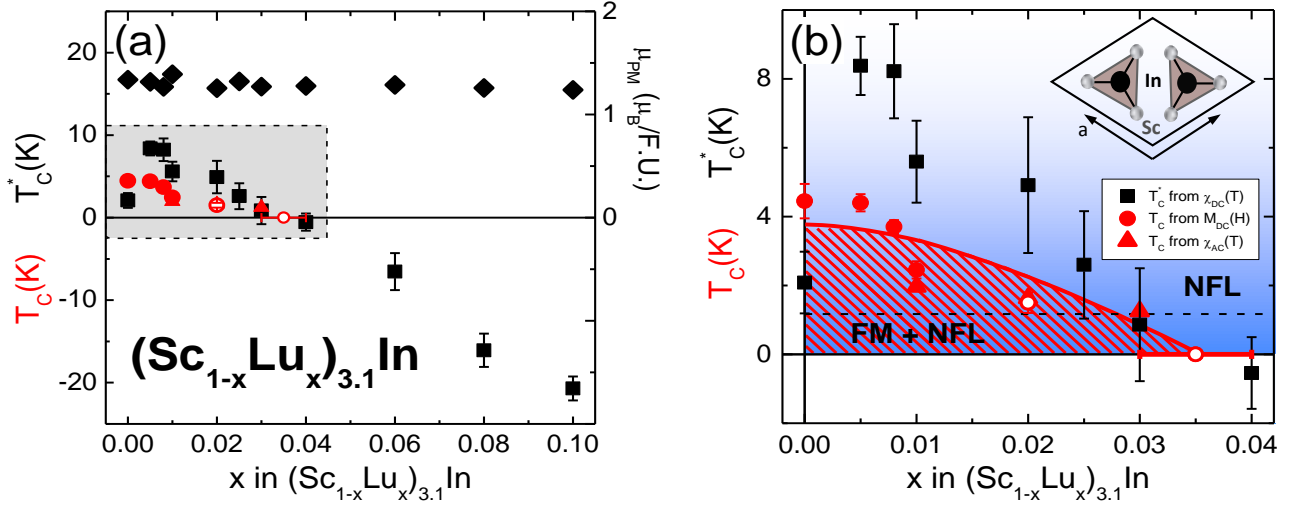


FIG. 13: (a) $T - x$ phase diagram for $(\text{Sc}_{1-x}\text{Lu}_x)_{3.1}\text{In}$ for $0 \leq x \leq 0.10$, with the Weiss-like temperature T_C^* (squares, left axis), the Curie temperature T_C (circles, left axis) and paramagnetic moment μ_{PM} (diamonds, right axis). (b) Enlarged $T - x$ phase diagram for $x \leq 0.04$ [shaded area in (a)], with the ab plane projection of the $\text{Sc}_{3.1}\text{In}$ unit cell shown in the inset. The horizontal line at $T = 1.17$ K denotes the minimum experimental temperature, with the open symbols representing T_C estimates extrapolated from accessible measurements.

Unveiling the quantum critical point of an Ising chain. *arXiv:1103.0095v1*, 2011.

- [5] D. J. W. Geldart and D. Neilson. Quantum critical behavior in the insulating region of the two-dimensional metal-insulator transition. *Physical Review B*, 76:193304, 2007.
- [6] Iulian Hetel, Thomas R. Lemberger, and Mohit Randeria. Quantum critical behavior in the superfluid density of strongly underdoped ultrathin copper oxide films. *Nature Physics*, 3:700, 2007.
- [7] D. A. Sokolov, M. C. Aronson, W. Gannon, and Z. Fisk. Critical phenomena and the quantum critical point of ferromagnetic $\text{Zr}_{1-x}\text{Nb}_x\text{Zn}_2$. *Physical Review Letters*, 96:116404, 2006.
- [8] A. Subedi and David J. Singh. Band structure and the itinerant magnetism in quantum critical NbFe_2 . *Physical Review B*, 81:024422, 2010.
- [9] H. Kadowaki, Y. Tabata, M. Sato, N. Aso, S. Raymond, and S. Kawarazaki. Quantum critical point of itinerant antiferromagnet in the heavy fermion. *Physical Review Letters*, 96:016401, 2006.
- [10] M. Yamada and S. Tanda. Quantum critical behavior in itinerant ferromagnet $\text{Pd}_{1-x}\text{Ni}_x$. *Physica B*, 284:1305, 2000.
- [11] A. Schroder, G. Aeppli, R. Coldea, M. Adams, O. Stockert, H.v Löhneysen, E. Bucher, R. Ramazashvili, and P. Coleman. Onset of antiferromagnetism in heavy-fermion metals. *Nature*, 407:351, 2000.
- [12] O. Trovarelli, C. Geibel, S. Mederle, C. Langhammer, F. M. Grosche, P. Gegenwart, M. Lang, G. Sparn, and F. Steglich. YbRh_2Si_2 : pronounces non-Fermi-liquid effects above a low-lying magnetic phase transition. *Physical Review Letters*, 85:626, 2000.
- [13] S. L. Bud'ko and P. C. Canfield. Field-induced quantum criticality in YbAgGe . *Physica B*, 403:1230, 2008.
- [14] S. Doniach. The kondo lattice and weak antiferromagnetism. *Physica B+C*, 91:231, 1977.
- [15] G. R. Stewart. Non-Fermi-liquid behavior in d- and f-electron metals. *Reviews of Modern Physics*, 73:797, 2001.
- [16] T. Moriya. Recent developments in the theory of spin fluctuations in itinerant electron magnets. *Physica B*, 86:356, 1977.
- [17] A. J. Millis. Effect of nonzero temperature on quantum critical points in itinerant fermion systems. *Physical Review B*, 48:7183, 1976.
- [18] M. Tsvelik and M. Reizer. Phenomenological theory of non-Fermi-liquid heavy-fermion alloys. *Physical Review B (R)*, 48:9887, 1993.
- [19] P. Gegenwart, Q. Si, and F. Steglich. Quantum criticality in heavy-fermion metals. *Nature Physics*, 4:186, 2008.
- [20] M. Continentino. On the zero temperature critical point in heavy fermions. *Physica B*, 101:197, 1996.
- [21] P. Coleman. Theories of non-Fermi liquid behavior in heavy fermions. *Phys. B*, 259:353, 1999.
- [22] W. Knafo, S. Raymond, J. Flouquet, B. Fak, M. A. Adams, P. Haen, F. Lapierre, S. Yates, and P. Lejay. Anomalous scaling behavior of the dynamical spin susceptibility of $\text{Ce}_{0.925}\text{La}_{0.075}\text{Ru}_2\text{Si}_2$. *Physical Review B*, 70:174401, 2004.
- [23] N. P. Butch and M. B. Maple. Evolution of critical scaling behavior near a ferromagnetic quantum phase transition. *Physical Review Letters*, 103:076404, 2009.
- [24] A. Aguayo and D. J. Singh. Itinerant ferromagnetism and quantum criticality in Sc_3In . *Physical Review B (R)*, 66:020401, 2002.
- [25] B. T. Matthias, A. M. Clogston, H. J. Williams, E. Corenzwit, and R. C. Sherwood. Ferromagnetism in solid solutions of scandium and indium. *Physical Review Letters*, 7:7, 1961.
- [26] W. E. Gardner, T. F. Smith, B. W. Howlett, C. W. Chu, and A. Sweedler. Magnetization measurements and pres-

- sure dependence of the Curie point of the phase Sc_3In . *Physical Review*, 166:577, 1968.
- [27] K. Ikeda and Jr. K. A. Gschneider. Disappearance of the heat capacity peak of Sc_3In around the Curie temperature in high magnetic fields. *Journal of Magnetism and Magnetic Materials*, 22:207, 1981.
- [28] J. Takeuchi and Y. Masuda. Low temperature specific heat of itinerant electron ferromagnet Sc_3In . *Journal of the Physical Society of Japan*, 46:468, 1979.
- [29] J. Grewe, J. S. Schilling, K. Ikeda, and Jr. K. A. Gschneider. Anomalous behavior of the weak itinerant ferromagnet Sc_3In under hydrostatic pressure. *Physical Review B*, 40:9017, 1989.
- [30] R. D. Shannon. Revised effective ionic radii and systematic studies of interatomic distances in halides and chalcogenides. *Acta Crystallographica*, 32:751, 1976.
- [31] V. B. Compton and B. T. Matthias. The crystal structure of Sc_3In . *Acta Crystallographica*, 15:94, 1962.
- [32] T. Jeong and Y. Kwon. Magnetism and electronic structure of $\text{Sc}_{3.1}\text{In}$. *Journal of the Korean Physical Society*, 51:629, 2007.
- [33] E. Svanidze, T. Besara, T. Siegrist, K. Han, and E. Morosan. in preparation.
- [34] A. Schenck. *Muon spin rotation spectroscopy principles and applications in solid state physics*. CRC Press, 1985.
- [35] S. L. Lee, S. H. Kilcoyne, and R. Cywinski. *Muon Science: Muons in Physics, Chemistry and Materials*. Taylor and Francis Group, 1999.
- [36] R. H. Heffner and K. Nagamine. Special issue on μSR : muon spin rotation, relaxation or resonance. *Journal of Physics: Condensed Matter*, 16:4403, 2004.
- [37] A. Yaouanc and P. Dalmas de Reotier. *Muon spin rotation, relaxation, and resonance: applications to condensed matter*. Oxford University Press, 2010.
- [38] J. E. Sonier. *MuSR brochure*. <http://musr.ca/intro/musr/muSRBrochure.pdf>, 2002.
- [39] T. Moriya. *Spin Fluctuations in Itinerant Electron Magnetism*. Springer - Verlag, Berlin, 1985.
- [40] A. Arrott. Criterion for ferromagnetism from observations of magnetic isotherms. *Physical Review*, 108:1394, 1957.
- [41] A. Arrott and J. E. Noakes. Approximate equation of state for nickel near its critical temperature. *Physical Review Letters*, 19:786, 1967.
- [42] E. D. Bauer, V. S. Zapf, P.-C. Ho, N. P. Butch, E. J. Freeman, C. Sirvent, and M. B. Maple. Non-Fermi-liquid behavior within the ferromagnetic phase in $\text{URu}_{2-x}\text{Re}_x\text{Si}_2$. *Physical Review Letters*, 94:046401, 2005.
- [43] A. H. Castro Neto and B. A. Jones. Non-Fermi-liquid behavior in U and Ce alloys: Criticality, disorder, dissipation, and Griffiths-McCoy singularities. *Physical Review B*, 62:14975, 2000.
- [44] R. B. Griffiths. Nonanalytical behavior above the critical point in a random Ising ferromagnet. *Physical Review Letters*, 23:1, 1969.
- [45] S. C. Abrahams. A neutron diffraction study of ZrZn_2 at 298 K and at 5 K. *Zeitschrift fur Kristallographie*, 112:427, 1959.
- [46] Y. J. Uemura, T. Goko, I. M. Gat-Malureanu, J. P. Carlo, P. L. Russo, A. T. Savici, A. Aczel, G. J. MacDougall, J. A. Rodriguez, and G. M. Luke. Phase separation and suppression of critical dynamics at quantum transitions of itinerant magnets: MnSi and $(\text{Sr}_{1-x}\text{Ca}_x)\text{RuO}_3$. *Nature Physics*, 3:29, 2007.
- [47] Y. J. Uemura, T. Yamazaki, D. R. Harshman, M. Senba, and E. J. Ansaldo. Muon-spin relaxation in AuFe and CuMn spin glasses. *Physical Review B*, 31:546, 1985.
- [48] I. M. Gat-Malureanu, J. P. Carlo, T. Goko, A. Fukaya, T. Ito, P. P. Kyriakou, M. I. Larkin, G. M. Luke, P. L. Russo, A. T. Savici, C. R. Wiebe, and K. Yoshimura nad Y. J. Uemura. Muon spin relaxation and susceptibility measurements of an itinerant-electron system $\text{Sr}_{1-x}\text{Ca}_x\text{RuO}_3$: quantum evolution from ferromagnet to paramagnet. *Physical Review B*, 84:224415, 2011.
- [49] J. P. Carlo, T. Goko, I. M. Gat-Malureanu, P. L. Russo, A. T. Savici, A. A. Aczel, G. J. MacDougall, J. A. Rodrigues, T. J. Williams, G. M. Luke, C. R. Wiebe, Y. Yoshida, S. Nakatsuji, Y. Maeno, T. Taniguchi, and Y. J. Uemura. New magnetic phase diagram of $(\text{Sr}, \text{Ca})_2\text{RuO}_4$. *Nature Materials*, 11:323, 2012.
- [50] Y. Nozaki, K. Nakanl, T. Yajima, H. Kageyama, B. Frandsen, L. Liu, S. Cheung, T. Goko, Y. J. Uemura, T. S. J. Munsie, T. Medina, G. M. Luke, J. Munevar, D. Nishio-Hamane, and C. M. Brown. Muon spin relaxation and electron/neutron diffraction studies of $\text{BaTi}_2(\text{As}_{1-x}\text{Sb}_x)_2\text{O}$: absence of static magnetism and superlattice reflections. *Physical Review B*, 88:214506, 2013.
- [51] R. S. Hayano, Y. J. Uemura, J. Imazato, N. Nishida, T. Yamazaki, and R. Kubo. Zero- and low-field spin relaxation studied by positive muons. *Physical Review B*, 20:850, 1979.